A dynamical system's approach to Schwarzschild null geodesics

2011 Class. Quantum Grav. 28 195007

(http://iopscience.iop.org/0264-9381/28/19/195007)

IOP PUBLISHING CLASSICAL AND QUANTUM GRAVITY

Class. Quantum Grav. **28** (2011) 195007 (13pp) doi:10.1088/0264-9381/28/19/195007

A dynamical system's approach to Schwarzschild null geodesics

Edward Belbruno[1,2] **and Frans Pretorius**[3]

[1] Courant Institute of Mathematical Sciences, New York University, NY, USA
[2] Princeton University, Princeton, NJ, USA
[3] Department of Physics, Princeton University, Princeton, NJ, USA

E-mail: belbruno@Princeton.EDU and fpretori@Princeton.EDU

Received 7 March 2011, in final form 19 July 2011
Published 7 September 2011
Online at stacks.iop.org/CQG/28/195007

Abstract

The null geodesics of a Schwarzschild black hole are studied from a dynamical system's perspective. Written in terms of Kerr–Schild coordinates, the null geodesic equation takes on the simple form of a particle moving under the influence of a Newtonian central force with an inverse-cubic potential. We apply a McGehee transformation to these equations, which clearly elucidates the full phase space of solutions. All the null geodesics belong to one of the four families of invariant manifolds and their limiting cases, further characterized by the angular momentum L of the orbit: for $|L| > |L_c|$, (1) the set that flow outward from the white hole, turn around, and then fall into the black hole, (2) the set that fall inward from past null infinity, turn around outside the black hole to continue to future null infinity, and for $|L| < |L_c|$, (3) the set that flow outward from the white hole and continue to future null infinity and (4) the set that flow inward from past null infinity and into the black hole. The critical angular momentum L_c corresponds to the unstable circular orbit at $r = 3M$, and the homoclinic orbits associated with it. There are two additional critical points of the flow at the singularity at $r = 0$. Though the solutions of geodesic motion and Hamiltonian flow we describe here are well known, what we believe is that a novel aspect of this work is the mapping between the two equivalent descriptions, and the different insights each approach can give to the problem. For example, the McGehee picture points to a particularly interesting limiting case of the class (1) that move from the white to black hole: in the $L \to \infty$ limit, as described in Schwarzschild coordinates, these geodesics begin at $r = 0$, flow along $t =$ constant lines, turn around at $r = 2M$, and then continue to $r = 0$. During this motion they circle in azimuth exactly once, and complete the journey in zero affine time.

PACS numbers: 04.20.−q, 04.70.Bw

(Some figures in this article are in colour only in the electronic version)

1. Introduction

The Schwarzschild metric, describing a static, non-rotating black hole solution to the Einstein field equations, was discovered within a year of Einstein's publication of the theory of general relativity. Though it had to wait till the 1960s before the full nature of the metric was truly uncovered, it has nevertheless been well studied for nearly a century. One of the more important tools in this regard is understanding the geodesic structure of the spacetime; in particular, timelike and null geodesics characterize the paths that a freely moving test particle P can follow within the spacetime. The geodesic equations of motion for P are a set of second order, ordinary differential equations, describing the evolution of the coordinates of P as a function of an affine parameter. In Schwarzschild, these equations are integrable, and the solutions have been known for a long time (see any standard text on general relativity). Nevertheless, the solutions exhibit a sufficiently rich set of dynamics that new insights into them are still being garnered. For example, in the past couple of decades dynamical system methods have been brought to bare on the geodesic equations, and perturbations thereof. A couple of the interesting results have been a new taxonomy of orbits based on the subset of orbits that are periodic, emphasizing the importance of the homoclinic orbits that asymptotically approach the unstable branch of circular orbits [1–3] and that a generic perturbation of the geodesic flow possesses a chaotic invariant set [4–10].

In this paper, we describe a new approach to understand the phase space of geodesic orbits, by applying a transformation due to McGehee [11].[4] This transformation is designed to resolve the singularities that formally appear in the Newtonian equations of motion when particles interacting through a central force collide. The transformation 'blows up' collision into an invariant manifold for the flow of the transformed differential equations. This allows the motion of P to be studied near collision, uncovering interesting dynamics. To apply these methods, we map the geodesic equation, written in Cartesian-like Kerr–Schild [13] (or ingoing Eddington–Finkelstein [14, 15]) coordinates, to a central force problem. This is trivial for the case where P has zero mass (null geodesic), which we focus on in this paper, though the methods can be generalized.

The rest of the paper is laid out as follows. In section 2, we introduce the Schwarzschild metric in the standard Schwarzschild coordinates, give an overview of its Penrose diagram and qualitatively discuss the null geodesics of the geometry. This will provide a point of reference as we map the geometric picture to a dynamical system's description within McGehee coordinates. In section 3, the differential equations for the motion of P are given, in Schwarzschild and Kerr–Schild coordinates. In section 4, we briefly summarize the results of the McGehee method for understanding the flow of a general class of Hamiltonian systems corresponding to central force problems. In section 5, we restrict to the particular system that maps to the null geodesic structure of Schwarzschild. We show that the phase space flow can be subdivided into four families of invariant manifolds and their limiting cases. There are four critical points of the flow—the black hole and white hole singularities at $r = 0$, and the two (with angular momentum $L = \pm L_c$) unstable circular orbits at $r = 3M$. Though much of the understanding of geodesic motion and the classical Hamiltonian system are individually well known, we believe that the novel aspect of this work is the (sometimes non-trivial) mapping between the two equivalent descriptions, and the insight one gives to the other. One particularly interesting example is the limiting case of geodesics that in the dynamical system's description flows 'directly' from the white to black hole: the collective set of these geodesics

[4] The McGehee transformation has been applied to the study of Schwarzschild geodesics before [12], though the focus of that study is largely orthogonal to ours; in particular, the connections between the Penrose and McGehee pictures as elucidated here were not drawn, which is the main emphasis of this work.

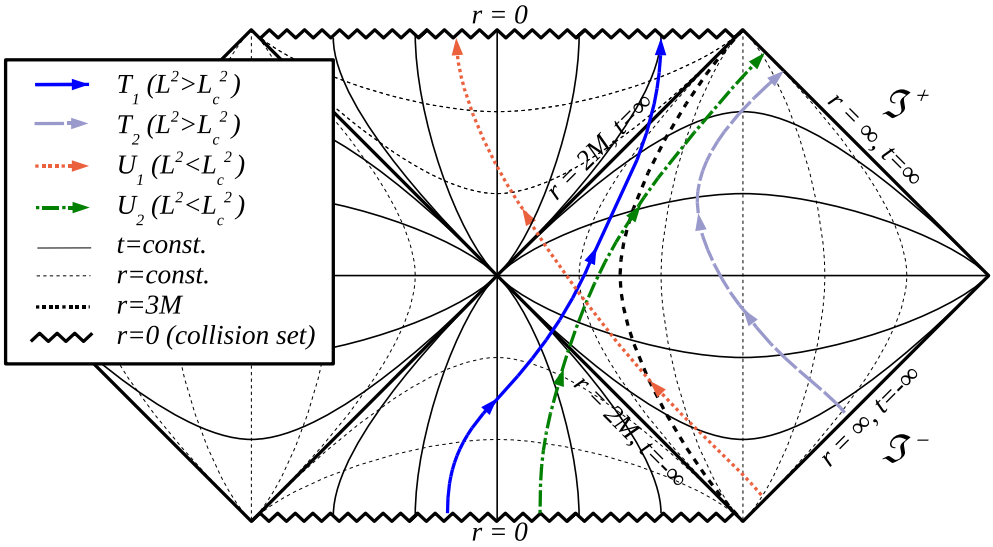

Figure 1. A schematic Penrose diagram of the Schwarzschild solution with representative null geodesics from each of the invariant manifolds; see figure 2 for the corresponding diagram in McGehee coordinates.

trace out the interior region of the white/black hole, flow along Schwarzschild t = const. lines, and complete exactly one orbit $\Delta\Phi = 2\pi$ along the journey from white hole to black hole singularity. Also, the standard affine parameter integrates to zero along these curves. To obtain a finite affine length requires rescaling it by an angular momentum-dependent quantity, which diverges in the limit. Details of all this are discussed in section 5, with some further comments in the conclusion, section 6. In section 6, we also provide a brief summary, and discussion of possible future extensions and applications. Throughout we use geometric units, where the speed of light $c = 1$ and Newton's constant $G = 1$.

2. The Schwarzschild geometry

The Schwarzschild metric, describing a non-rotating black hole of mass M, has the following line element in standard (spherical polar) Schwarzschild coordinates:

$$ds^2 = g_{\alpha\beta}\,dx^\alpha\,dx^\beta = -(1-2M/r)\,dt^2 + (1-2M/r)^{-1}\,dr^2 + r^2(d\theta^2 + \sin^2\theta\,d\phi^2), \qquad (1)$$

where $g_{\alpha\beta}$ is the metric tensor, and we use the Einstein summation convention where repeat indices are summed over. Figure 1 shows a Penrose diagram of the Schwarzschild spacetime. For readers not familiar with this diagram, we will briefly review its salient features. The Penrose diagram is a conformal compactification of the maximal analytic extension of the Schwarzschild metric, designed to highlight the causal structure of the spacetime. Here we project out the (θ, ϕ) coordinates, so a point in the diagram represents a two-sphere of area $4\pi r^2$. Radial (zero angular momentum) null geodesics are straight lines angled at $\pm 45^\circ$ relative to the horizontal. Any causal curve that could be associated with a particle trajectory (whether timelike, null, geodesic or not) has a slope $\geqslant 45^\circ$ *everywhere* along its projected curve on the diagram. There are two identical, causally disconnected, asymptotically flat regions reached as $r \to \infty$; without loss of generality, we focus on the right-hand region of the diagram. Similarly, there are two singularities in the geometry at $r = 0$: the *white hole*

singularity occurring to the past of any event in the spacetime, and the *black hole* singularity that is within the causal future of any event.

A null curve can be parameterized by an affine time σ, unique up to a constant scaling and translation. Null curves that originate at $r = \infty$ (with $\sigma \to -\infty$) come from a region called *past null infinity* $\Im^-$, and those that return to $r = \infty$ (as $\sigma \to +\infty$) end at *future null infinity* $\Im^+$. The event horizon of the black hole is formally defined as the boundary of the causal part of $\Im^+$, which on the Penrose diagram is the line labeled $r = 2M, t = \infty$. Null curves that come from the white hole 'begin' at $r = 0$ with finite σ, and those that cross the event horizon reach $r = 0$ in finite affine time. Note that the Schwarzschild time coordinate t is singular at $r = 2M$. Further, note that r and t switch 'character' at $r = 2M$: outside, r is spacelike, t is timelike and vice versa inside. In the black hole, time as measured by r flows to smaller r (the opposite in the white hole). Thus, the inevitability of encountering the singular at $r = 0$ for any observer crossing the horizon is evident in the diagram: $r = 0$ is no longer a 'place' that can be avoided, rather it is a 'time' that will happen for any such observer. Finally, note that the compactification severely distorts the spacetime at the corner points of the diagram—that $r = 0$, $r = 2M$ and $r = \infty$ touch in the diagram is purely an artifact of the compactification.

3. Geodesic equations in the Schwarzschild spacetime

We begin by describing the geodesic equations for causal particles; later, we restrict to the null case. The geodesic equation for a particle P in the parametric form $x^\alpha(\sigma)$ is

$$\ddot{x}^\alpha + \Gamma^\alpha_{\beta\gamma}\dot{x}^\beta\dot{x}^\gamma = 0, \tag{2}$$

where the over-dot $\dot{} \equiv \mathrm{d}/\mathrm{d}\sigma$ and $\Gamma^\alpha_{\beta\gamma}$ is the metric connection. This is formally a set of second order ordinary differential equations, though due to the symmetries of the Schwarzschild metric, and the normalization condition that $g_{\alpha\beta}\dot{x}^\alpha\dot{x}^\beta$ equals 0 (-1) for null (timelike) geodesics, one obtains the following first integrals of motion of (2) in Schwarzschild coordinates (1):

$$\begin{aligned}
&\dot{t} = \tilde{E}(1 - 2M/r)^{-1}\\
&r^4\dot{r}^2 = \tilde{E}^2r^4 - (r^2 - 2Mr)(\mu^2r^2 + K)\\
&r^4\dot{\theta}^2 = K - L^2\sin^{-2}\theta\\
&\dot{\phi} = L(r^2\sin^2\theta)^{-1},
\end{aligned} \tag{3}$$

where μ^2 is the rest mass of P, $\tilde{E}$ is its energy, L is its angular momentum about the axis $\sin\theta = 0$, and K is Carter's constant of motion. Note that the second equation above for $\dot{r}$ can be written as a Newtonian central force problem

$$E = \tfrac{1}{2}\dot{r}^2 + V(r), \tag{4}$$

with equation of motion

$$\ddot{r} = -\mathrm{d}V/\mathrm{d}r, \tag{5}$$

where $E = \tilde{E}^2/2$ and the effective potential $V(r)$ is given by

$$V(r) = \frac{1}{2}\left(1 - \frac{2M}{r}\right)\left(\mu^2 + \frac{K}{r^2}\right). \tag{6}$$

Kerr–Schild coordinates

The Schwarzschild metric in Cartesian Kerr–Schild coordinates (λ, x, y, z) is

$$\mathrm{d}s^2 = -\mathrm{d}\lambda^2 + \mathrm{d}x^2 + \mathrm{d}y^2 + \mathrm{d}z^2 + 2Mr^{-3}(x\,\mathrm{d}x + y\,\mathrm{d}y + z\,\mathrm{d}z + r\,\mathrm{d}\lambda)^2, \tag{7}$$

related to Schwarzschild coordinates by the set of transformations

$$x = r\sin\theta\cos\phi, \qquad y = r\sin\theta\sin\phi, \qquad z = r\cos\theta \tag{8}$$

and

$$\mathrm{d}\lambda = \mathrm{d}t + \frac{2M}{r-2M}\,\mathrm{d}r. \tag{9}$$

One advantage of Kerr–Schild coordinates over Schwarzschild coordinates, as is evident from (7), is that they are regular across the event horizon at $r = 2M$.[5]

The geodesic equations in Kerr–Schild coordinates can be written as [16]

$$\dot{\lambda} = 2MKr^{-3}(\tilde{E} - \dot{r})^{-1} + \tilde{E} \tag{10}$$

$$\ddot{x}_k = -3MKx_k r^{-5} - \mu^2 M x_k r^{-3}, \tag{11}$$

where for the sake of notation, $k = 1, 2, 3$, with $x_1 = x$, $x_2 = y$, $x_3 = z$. Due to the spherical symmetry of the Schwarzschild spacetime, without loss of generality we can restrict attention to planar motion. For simplicity, we choose $z = 0$, corresponding to $\theta = \pi/2$ for which $K = L^2$ (3). In the expressions below, we will replace K with L^2, though one can consider them to be valid for motion in any plane if L is re-interpreted as the angular momentum relative to an axis orthogonal to the orbital plane. We will also now limit the discussion to null geodesics for which $\mu^2 = 0$, and only focus on the coordinate flow (11) of the geodesics:

$$\ddot{\mathbf{x}} = -3ML^2\mathbf{x}r^{-5}, \tag{12}$$

where $\mathbf{x} = (x_1, x_2) \in R^2$ and $r = |\mathbf{x}| = \sqrt{x_1^2 + x_2^2}$.

The corresponding Hamiltonian for this system of equations is

$$E = H(\mathbf{x}, \dot{\mathbf{x}}) = \tfrac{1}{2}|\dot{\mathbf{x}}|^2 - L^2 M|\mathbf{x}|^{-3}, \tag{13}$$

where $E = \tilde{E}^2/2$ is a positive constant of motion for any particle trajectory.

It is noted that for each value $h \geqslant 0$ of the energy E, the motion of P of mass zero lies on the three-dimensional energy surface

$$\Sigma = \{(\mathbf{x}, \dot{\mathbf{x}}) \in R^4 | H(\mathbf{x}) = h \geqslant 0\}. \tag{14}$$

To facilitate direct application of prior work on Newtonian central force problems of the form (12), it is useful to perform the following *dimensionful* rescaling of the affine parameter σ to ξ:

$$\sigma = \frac{\xi}{\sqrt{L^2 M}}. \tag{15}$$

This transforms (12) into

$$\frac{\mathrm{d}^2\mathbf{x}}{\mathrm{d}\xi^2} = -3\mathbf{x}r^{-5}. \tag{16}$$

In the following section, we consider the solutions $\mathbf{x}(\xi) = (x_1(\xi), x_2(\xi))$ of (16).

[5] Technically, (7) is only regular across the black hole event horizon, and not the Cauchy horizon at $r = 2M$ of the white hole. The reason is that λ has been chosen so that along an $r =$ const. surface, λ coincides with the retarded time v of an *ingoing* radial null curve coming from $\Im^-$, and $v \to -\infty$ as the white hole horizon is approached in the Penrose diagram. These coordinates are thus also referred to as ingoing Eddington–Finkelstein coordinates. If instead we had chosen a coordinate $\bar{\lambda} = \mathrm{d}t - 2M/(r-2M)\mathrm{d}r$, then $\bar{\lambda}$ would coincide with advanced time u of an outgoing radial photon along an $r =$ const. surface (outgoing Eddington–Finkelstein coordinates), and the metric would be regular at the white hole horizon, but singular at the black hole horizon for similar reasons. However, at the end of the day, one arrives at the *same* geodesic equation of interest (12) for the spatial Cartesian coordinates as a function of *affine time* $[x(\sigma), y(\sigma), z(\sigma)]$, which is well defined across both horizons.

4. Transformation to McGehee coordinates and blowup of collision

We consider general central force fields with the potential

$$U(\mathbf{x}) = -|\mathbf{x}|^{-\alpha}, \tag{17}$$

$\alpha > 0$, later restricting to the case $\alpha = 3$ of (16). The system of differential equation describing the motion of a single particle with this potential is given by

$$\ddot{\mathbf{x}} = -\partial_{\mathbf{x}} U(\mathbf{x}) = -\alpha|\mathbf{x}|^{-\alpha-2}\mathbf{x}. \tag{18}$$

It is convenient to write this as the first-order system

$$\begin{aligned} \dot{\mathbf{x}} &= \mathbf{y}, \\ \dot{\mathbf{y}} &= -\alpha|\mathbf{x}|^{-\alpha-2}\mathbf{x}. \end{aligned} \tag{19}$$

This is a Hamiltonian system with the Hamiltonian function

$$H(\mathbf{x}, \mathbf{y}) = \tfrac{1}{2}|\mathbf{y}|^2 - |\mathbf{x}|^{-\alpha}, \tag{20}$$

which is the total energy of the particle and is conserved along solutions of (19), where $(\mathbf{x}, \mathbf{y}) \in R^4$.

The general description of the orbit structure for (19) was carried out in [11], with a special emphasis on the motion of the particle near collision. The general approach taken is to find a change of coordinates which have the effect of blowing up the collision, corresponding to $\mathbf{x} = \mathbf{0}$, into an invariant manifold with its own flow. When this is done, the dynamics of the particle near collision can be completely understood and solutions tending toward collision are asymptotic to this manifold. This change of coordinates also gives the global flow for the differential equations.

Set $\mathbf{X} = (\mathbf{x}, \mathbf{y})$, and consider a solution $\mathbf{X}(\xi) = (\mathbf{x}(\xi), \mathbf{y}(\xi))$ for (19) with an initial condition $\mathbf{X}(0)$. The standard existence and uniqueness theorems of differential equations guarantee that $\mathbf{X}(\xi)$ can be uniquely determined and defined over a maximal interval (ξ^-, ξ^+), where $-\infty \leqslant \xi^- < 0 < \xi^+ \leqslant +\infty$.

Definition. *If $\xi^+ < \infty$, then $\mathbf{X}(\xi)$ ends in a singularity at ξ^+. If $\xi^- \geqslant -\infty$, then $\mathbf{X}(\xi)$ begins in a singularity at ξ^-. In either case, $\xi^* = \xi^+$ or ξ^- is said to be a singularity of the solution $\mathbf{X}(\xi)$.*

The following result is proven in [11].

Let $\mathbf{X}(\xi)$ be a solution of (19) with a singularity at ξ^*. Then, this singularity is due to collision. That is, $\mathbf{x}(\xi) \to 0$ as $z \to \xi^*$.

It follows from (20) that for a collision solution, $|\mathbf{y}| \to \infty$ as $z \to \xi^*$. Hence, for (19) the only solutions that are singular are collision solutions, either ending or beginning in collision. There are several methods available to study collision, the dynamics of solutions near it and to understand if a collision solution can be extended through the collision state in a continuous fashion. Here we present a brief summary of blowing up collision for (19) for arbitrary $\alpha > 0$, and then apply that to understand the global flow for the case of $\alpha = 3$. The details are in [11].

We set $\beta = \frac{\alpha}{2}$, $\gamma = (1+\beta)^{-1}$ for the sake of notation. Also, it is convenient to use complex coordinates and identify the real plane R^2 with the complex plane C^1. Then, we can consider $\mathbf{x}$ to be a vector in R^2 or a complex number in C^1. The *McGehee coordinates* are given by the transformation T of (x_1, x_2, y_1, y_2) to $(\tilde{r} > 0, \tilde{\theta}, w, v)$:

$$\begin{aligned} \mathbf{x} &= \tilde{r}^{\gamma} \mathrm{e}^{\mathrm{i}\tilde{\theta}} \\ \mathbf{y} &= \tilde{r}^{-\beta\gamma} (v + \mathrm{i}w)\, \mathrm{e}^{\mathrm{i}\tilde{\theta}} \end{aligned} \tag{21}$$

and a transformation of the affine variable ξ,

$$d\xi = \tilde{r} d\tau. \tag{22}$$

The system (19) is transformed into

$$\begin{aligned} \tilde{r}' &= (\beta + 1)\tilde{r}v, \\ \tilde{\theta}' &= w, \\ w' &= (\beta - 1)wv, \\ v' &= w^2 + \beta(v^2 - 2), \end{aligned} \tag{23}$$

where prime denotes differentiation w.r.t. τ. In the complex notation, the angular momentum for (19) is given by

$$\Omega(\mathbf{x}, \mathbf{y}) = \Im(\bar{\mathbf{x}}\mathbf{y}). \tag{24}$$

We fix the energy H to the constant value h and Ω to the constant value c (not to be confused with the speed of light). T transforms $H = h$ and $\Omega = c$ into

$$w^2 + v^2 - 2 = 2h\tilde{r}^{\alpha\gamma} \tag{25}$$

$$\tilde{r}^{(1-\beta)\gamma} w = c. \tag{26}$$

We define the constant energy manifold,

$$\mathbf{M}(h) = \{(\tilde{r}, \tilde{\theta}, w, v) \in R^4 | \tilde{r} \geqslant 0, H = h\}. \tag{27}$$

We define the collision set corresponding to collisions for the system (19) as

$$\mathbf{N} = \{(\tilde{r}, \tilde{\theta}, w, v) \in \mathbf{M}(h) | \tilde{r} = 0\}. \tag{28}$$

On account of (25), (26) and (28) can be written as

$$\mathbf{N} = \{(\tilde{r}, \tilde{\theta}, w, v) \in \mathbf{M}(h) | \tilde{r} = 0, v^2 = 2, w = 0\} \quad \beta > 1, \tag{29}$$

$$\mathbf{N} = \{(\tilde{r}, \tilde{\theta}, w, v) \in \mathbf{M}(h) | \tilde{r} = 0, v^2 + c^2 = 2, w = c\} \quad \beta = 1, \tag{30}$$

$$\mathbf{N} = \{(\tilde{r}, \tilde{\theta}, w, v) \in \mathbf{M}(h) | \tilde{r} = 0, w^2 + v^2 = 2, c = 0\} \quad 0 < \beta < 1. \tag{31}$$

As is proven in [11],

N is an invariant manifold for the vector field defined by the system (23). Collision orbits approach **N** asymptotically as $\tau \to \pm\infty$.

Definition. **N** *is called a blowup of the collision* $\tilde{r} = 0$ *on* $\mathbf{M}(h)$.

It is also shown in [11] that the system (23) reduces to the system consisting of the last two equations of (23),

$$\begin{aligned} w' &= (\beta - 1)wv, \\ v' &= w^2 + \beta(v^2 - 2). \end{aligned} \tag{32}$$

This system has the integral

$$\Lambda(w, v) = |w|^{\alpha} |v^2 + w^2 - 2|^{1-\beta}. \tag{33}$$

In summary, to understand the flow of (19) on $\mathbf{M}(h)$, we can use the system (32), where the collision manifold is given by **N**.

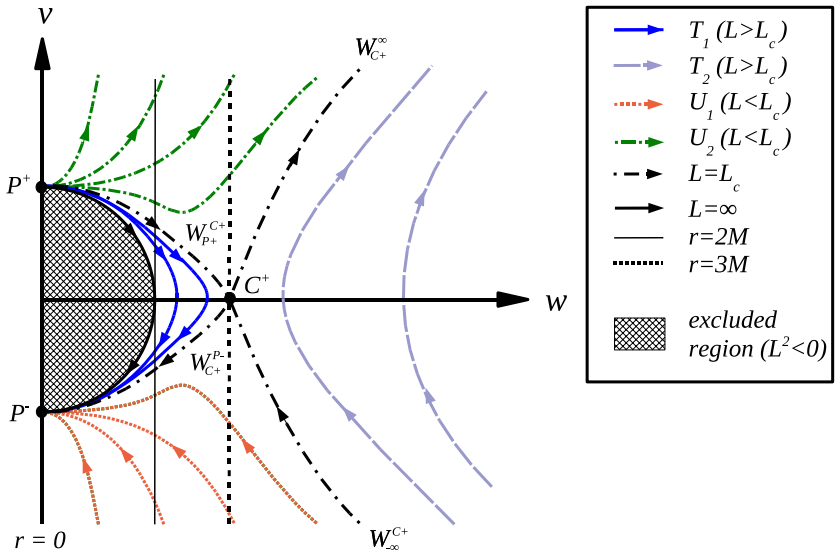

Figure 2. The Schwarzschild null geodesic flow in McGehee coordinates; see figure 1 for the corresponding Penrose diagram. The point P^- (P^+) here corresponds to the black hole (white hole) singularity at $r = 0$. For clarity, we only show the half-plane $w > 0$, corresponding to positive angular momentum L orbits; the flow in $w < 0$ for negative angular momentum orbits looks identical to that of $w > 0$, but reflected about the v axis.

5. McGehee flow of Schwarzschild null geodesics

We now consider the case of interest given by the Schwarzschild problem that we showed reduced to the system (16). This corresponds to $\alpha = 3$, $\beta = 3/2$, $\gamma = 2/5$. The flow for system (32) is depicted in figure 2. Incidentally, this figure captures the qualitative behavior for all values of $\beta > 1$. It turns out that the flows for $\beta \leqslant 1$ are drastically different; in particular, the Kepler problem corresponds to $\beta = 1/2$. Over the next several paragraphs, we will describe the flow in some detail, though first it would be helpful to identify a few relations between the coordinates (w, v) and physical coordinates, as well as establish the map between the constants of motion (h, c) of solutions to the system (19) and the physically relevant constants L, $\tilde{E}$ and M.

Relationships between constants and coordinates. Using (21) and (26), and the angular momentum of the geodesic in the physical picture $L = x\dot{y} - y\dot{x}$, one finds that the angular momentum c of the system (19) evaluates to

$$c = \pm\frac{1}{\sqrt{M}}. \tag{34}$$

This rather unusual relationship is due to the scaling (15) between the time parameters of the two descriptions. Likewise, it is straightforward to show that the energy h of the system (19) relates to physical constants via

$$h = \frac{\tilde{E}^2}{2L^2M}. \tag{35}$$

From (21), the relation between the areal radius r and $\tilde{r}$ for $\alpha = 3$ is

$$r = \tilde{r}^{2/5}, \tag{36}$$

and this together with (34) and (26) gives

$$w = \pm\sqrt{\frac{r}{M}}, \tag{37}$$

where the plus (minus) sign corresponds to positive (negative) physical angular momentum L. Thus, vertical lines of constant w on the McGehee diagram correspond to surfaces of constant areal radius r. Putting all the above together, with (25), one finds that all trajectories projected onto the (w, v) plane are characterized by the following polynomial with one free parameter $Q \geqslant 0$:

$$v^2 = 2 - w^2 + Qw^6, \tag{38}$$

$$Q \equiv \frac{\tilde{E}^2 M^2}{L^2}. \tag{39}$$

Finally, note from (23) that $v = 0$ implies $\tilde{r}' = 0$, which translates into $\dot{r} = 0$; thus, a trajectory that crosses $v = 0$ corresponds to a geodesic that has a turning point in its radial motion.

Particle flow. Figure 2 is a projection of the full flow in $(\tilde{r}, \tilde{\theta}, w, v)$ coordinates to the (w, v) plane. Though as seen in (23), the two differential equations for (w', v') do not depend on $(\tilde{r}, \tilde{\theta})$ and can be solved separately as an independent system. Once we know (w, v), the coordinates $(\tilde{r}, \tilde{\theta})$ can be easily computed for each (w, v) by (23). ($\tilde{\theta}$ and $\tilde{r}$) represent polar-like coordinates for P, while (w, v) can be viewed as velocity-like coordinates. The system (23) implies that $\tilde{\theta}(\tau)$ either increases, $w > 0$, or decreases, $w < 0$. This is just a cycling motion about the origin $\tilde{r} = 0$ in position coordinates $\tilde{r}, \tilde{\theta}$. While this cycling motion is occurring, $\tilde{r}$ increases, $v > 0$, or decreases, $v < 0$. This is analogous to the projection on the Penrose diagram of the flow in (r, t, θ, ϕ) to the (conformally compactified) (r, t) plane, and the cyclic motion for $K = L^2$ geodesics corresponds to increasing ϕ, $L > 0$, or decreasing ϕ, $L < 0$.

The flow curves $(w(\tau), v(\tau))$ in figure 2 can be viewed as invariant manifolds. They foliate the (w, v)-plane. From (23), one can see that the flow has critical points $C^{\pm}$ at $(w, v) = (\pm\sqrt{3}, 0)$, where $\tilde{r} = \sqrt{3}$ and $\tilde{\theta} = \pm\sqrt{3}\tau$ (to within a constant phase), respectively. These correspond to the unstable (hyperbolic) circular periodic orbits at $r = 3M$. The periodic orbits $C^{\pm}$ exist for each $h > 0$ on each energy surface $\mathbf{M}(h)$.

Excluded region. The flow on $\mathbf{M}(h)$ for (32) projects into the set $\{w^2 + v^2 \leqslant 2\}$ for each $h < 0$, into $\{w^2 + v^2 = 2\}$ for $h = 0$ and into $\{w^2 + v^2 > 2\}$ for $h > 2$. Hence, since P moves on Σ, defined by (14), where $h \geqslant 0$, we need not consider the interior of the disk, $\{w^2 + v^2 < 2\}$. So, in figure 2, the region of interest is all points $\{w^2 + v^2 \geqslant 2\}$.

The collision set. The collision set $\mathbf{N}$ for $\alpha = 3$ reduces to two critical points of the flow, $p^+ = (0, \sqrt{2})$ and $p^- = (0, -\sqrt{2})$. These are unstable hyperbolic points. The flow tends to p^+ as $\tau \to -\infty$ and to p^- as $\tau \to +\infty$. In the full phase space, these critical points have a constant value of $\tilde{\theta}$ and $\tilde{r} = 0$. On the Penrose diagram, p^- (p^+) corresponds to the black hole (white hole) singularity at $r = 0$.

Invariant manifolds of the flow. There are invariant manifolds connecting $C^{\pm}$ and $p^{\pm}$. Two flow from p^+ to $C^{\pm}$ and two flow from $C^{\pm}$ to p^-. These are labeled as $W^{C^{\pm}}_{p^+}$ and $W^{p^-}_{C^{\pm}}$, respectively; trajectories within this flow have physical angular momentum squared $L_c^2 = 27\tilde{E}^2 M^2$. As P moves along, e.g. $W^{C^+}_{p^+}$, it can be viewed in position space as cycling

about the origin while moving outward toward the periodic orbit. The cycles converge to the periodic orbit asymptotically as $\tau \to \infty$ for $W^{C^+}_{p^+}$, and $\tau \to -\infty$ for $W^{p^-}_{C^+}$.

There are curves that leave p^+, move out to a maximum distance within the range $\sqrt{2} < w < \sqrt{3}$ ($2M < r < 3M$) when $v = 0$, and then turn around and move to p^-. We label these manifolds $W^{p^-}_{p^+}$, and all of these geodesics have $L^2 > L^2_c$. The union of these manifolds fill a region labeled T_1 in figure 2. In the limit $L \to \pm|L_c|$, the solutions asymptote to the union of $W^{C^\pm}_{p^+}$ and $W^{p^-}_{C^\pm}$. The $L^2 \to \infty$ limit ($h \to 0$) is a rather interesting class of geodesics, which we discuss in the following subsection.

Similarly, we have solutions that come in from negative infinity ($\Im^-$) for $v < 0$, reach a minimum distance from the black hole in the range $w > \sqrt{3}$ ($r > 3M$) when $v = 0$, and then go back out to positive infinity ($\Im^+$) with $v > 0$; they lie on invariant manifolds called $W^{+\infty}_{-\infty}$, and are labeled T_2 in figure 2. As with T_1, all these geodesics have angular momentum squared $L^2 > L^2_c$. In the limit $L \to \pm|L_c|$, they asymptote to the union of the manifolds $W^{C^\pm}_{-\infty}$ and $W^{\infty}_{C^\pm}$, the manifolds that connect $\Im^-$ to $C^\pm$ and $C^\pm$ to $\Im^+$, respectively. The solutions on $W^{C^\pm}_{-\infty}$ asymptotically ($\tau \to \infty$) approach the circular orbit as they spiral toward it from $\Im^-$, and those on $W^{\infty}_{C^\pm}$ (beginning at $\tau = -\infty$) asymptotically spiral away from the circular orbit to $\Im^+$.

The remaining two regions of the flow are called U_1 and U_2. U_1 consists of the manifolds $W^{p^-}_{-\infty}$, which spiral in from $\Im^-$ into the black hole. They do not encounter a turning point in r. These geodesics all have $L^2 < L^2_c$, and in the limit $L \to \pm|L_c|$ asymptotically approach the union of manifolds $W^{C^\pm}_{-\infty}$ and $W^{p^-}_{C^\pm}$. Similarly, U_1 consists of the manifolds $W^{\infty}_{p^+}$, which spiral out from the white hole to $\Im^-$, do not have a turning point in r, have $L^2 < L^2_c$, and in the limit $L \to \pm|L_c|$ asymptote to the union of $W^{C^\pm}_{p^+}$ and $W^{\infty}_{C^\pm}$.

The $L^2 \to \infty$ ($h = 0$) limit. In the region T_1, geodesics with $h \to 0$ correspond to the limit $\ell^2 \equiv L^2/\tilde{E}^2 \to \infty$. Fixing the physical energy $\tilde{E}$ to be finite, these geodesics have several curious properties[6], most easily deduced from the geodesic equations in Schwarzschild coordinates (3). First, for $r \leqslant 2M$,

$$\frac{\mathrm{d}t}{\mathrm{d}r} = \pm \frac{r^{3/2}}{\sqrt{r(2M-r)^2 + \ell^2(2M-r)}}, \tag{40}$$

where the $+(-)$ sign corresponds to the part of the trajectory in the white (black) hole where $\dot{r} > 0$ ($\dot{r} < 0$). Taking the limit $\ell \to \infty$, one gets that these geodesics projected onto the (r, t) plane in the Penrose diagram correspond to $t =$ constant lines (and recall that inside the horizon t is a spacelike coordinate), i.e. they emanate from the white hole singularity, turn around at the intersection of the event and Cauchy horizons at $r = 2M$, and then continue to the black hole singularity. Next, we calculate how much cycling motion in ϕ they execute. From the geodesic equations,

$$\frac{\mathrm{d}\phi}{\mathrm{d}r} = \pm \frac{\ell}{\sqrt{r^4 + r\ell^2(2M-r)}}, \tag{41}$$

again where $+(-)$ corresponds to the white (black) hole regions. Taking the limit $\ell \to \infty$, and integrating from $r = 0$ to $2M$ in the white hole and back from $r = 2M$ to 0 in the black hole,

[6] In contrast to the $\ell^2 \to \infty$ limit region of T_2, which simply corresponds to geodesics that pass by the black hole with an infinite impact parameter.

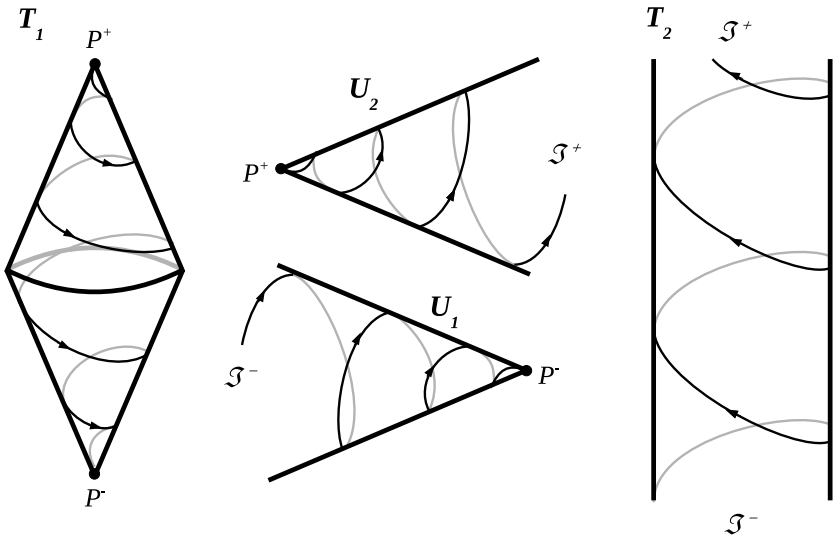

Figure 3. Topology of the flow traced out by solutions within each of the four invariant manifolds T_1, T_2, U_1 and U_2 (see figure 2). Note that the sample trajectories are schematic only and for visual aid; only those solutions that flow close to the critical points $C^{\pm}$ trace out multiple cycles, and these are clustered near $w = \sqrt{3}$ ($r = 3M$).

gives $|\Delta\Phi| = 2\pi$ for the journey—these geodesics circle in azimuth exactly *once* going from the white to black hole singularity. Finally, we compute the total affine time $\Delta\sigma = \int \mathrm{d}\sigma$ from

$$\frac{\mathrm{d}\sigma}{\mathrm{d}r} = \pm\frac{r^{3/2}}{\tilde{E}\sqrt{r^3 + \ell^2(2M - r)}}. \tag{42}$$

For finite $\tilde{E}$, in the limit $\ell \to \infty$, $\Delta\sigma = 0$! This rather bizarre result could be remedied by an infinite rescaling of $\sigma \to \sigma(\ell_0/\ell)$, where ℓ_0 is some finite constant with the dimension of length to make the scaling dimensionless. It is unclear what the physical significance of such a rescaling is. Further discussion of this limiting case is relegated to the conclusion.

Topology of the flow. The solutions in the flow T_1 that spiral out from the white hole turn around at $\sqrt{2} \leqslant w \leqslant \sqrt{3}$, and return to the black hole, trace out surfaces that are topologically equivalent to two cones smoothly joined together at $v = 0$, with vertices anchored in the critical points at p^+, $p-$; see figure 3. The flows U_1 coming from $\Im^-$ into the black hole topologically form an (infinite length) open cone, with the open end at $\Im^-$, and the vertex at p^+; similarly for the flows in U_2. The geodesics in T_2 that come in from $\Im^-$ and return to $\Im^+$ lie on families of surfaces that are topologically equivalent to (infinite) cylinders.

Extension of solutions through collision. Let $\mathbf{x}(\xi)$ be any solution of (18) which ends in collision at $\xi = 0$. That is, $\mathbf{x}(\xi) \to 0$ as $\xi \to 0_-$, where $\xi \to 0_-$ means that ξ approaches 0 where $\xi < 0$. It is proven in [11] that $\mathbf{x}(\xi)$ is *branch regularizable* if and only if $\gamma \in \Xi$, where we define the set Ξ as follows. Let m, n be relatively prime integers; then, $\Xi = \{m/n | n \text{ odd}, n > m > 0\}$. Recall that $\gamma = (1 + \beta)^{-1}$, $\alpha = 2\beta$. In our case, $\alpha = 3$ and $\gamma = 2/5$ belong to the set Ξ.

The fact that $\mathbf{x}(\xi)$ is branch regularizable implies that there is a way that solutions can continuously and *uniquely* be extended through p^+ backward in time and through p^- forward

in time. For example, let $\mathbf{Z}(\xi) = (\mathbf{x}(\xi), \mathbf{y}(\xi))$ be a trajectory in phase space defined for $\xi < 0$ that collides with p^- at $\xi = 0$. Then there exists a unique extension of $\mathbf{Z}(\xi)$ for $\xi > 0$. This extension is real analytic as a function of ξ and corresponds to a bounce of P in the (x_1, x_2) space. In the spacetime picture, collision with p^- corresponds to the geodesic encountering the black hole singularity. The field equations of general relativity do not describe how spacetime can be extended beyond a singularity, and it is usually thought that a theory of quantum gravity is required to 'resolve' the singularity. Nevertheless, one way to map the branch-regularized extension to geodesic motion 'through' the singularity would be to identify the black hole singularity with a white hole singularity of a second Schwarzschild solution of identical mass[7].

6. Conclusions

In this paper, we have studied the relationship between the null geodesic structure of the Schwarzschild black hole solution, and the corresponding inverse-cubic Newtonian central force problem, using the methods of McGehee. Both these problems have been well studied before, though what we believe is novel in this paper is highlighting the *exact* correspondence between the two descriptions, allowing insights from the dynamical system's approach to be brought to the geodesic problem, and vice versa. Indeed, in that regard, it is rather amusing to note that McGehee titled his paper 'Double Collisions for Classical Particle System with Nongravitational Interactions'. It is also rather interesting that what in the Newtonian picture may be regarded as a clever 'trick' using coordinate transformations to blow up the singular point of collision between two particles is in a sense the natural way to describe Schwarzschild spacetime. And though the result of this mapping, as depicted in figures 1 and 2, is rather simple in the end, the intermediate steps required are not trivial. For example, the dimensionful scaling of parameters that put the geodesic picture in a form that one can directly apply McGehee's results to is a bit bizarre and unobvious. As a case in point, what in the dynamical system's picture is an arbitrary conserved angular momentum constant c is now restricted to take on exactly the values $c^2 = 1/M$, and is completely unrelated to the physical angular momentum L of geodesics.

We would also like to make a few additional comments on the $L \to \infty$ limit discussed in section 5. There, we noted that the 'usual' definition of the affine time led to a geodesic with zero integrated affine time for the journey from the white to black hole. A different conclusion could be reached if we allowed the energy $\tilde{E}$ to be zero. However, this does not seem to be physically reasonable if one invokes the standard relationship between null geodesics and photons. Then, the physical energy measured by a local observer is proportional to the wavelength of the photon, which can be related to the integration constant $\tilde{E}$. Demanding that this be positive-definite restricts to the subset of real photons that can be observed in 'our' (the right-side) universe within the Penrose diagram. Furthermore, the wavelength of the photon is inversely proportional to $\tilde{E}$; thus, the limit $\tilde{E} \to 0$ corresponds to infinite wavelength photons, which does not seem to be a limit of physical relevance to photons confined to a small region about the white hole/black hole.

A further concern about the unusual properties of the $L \to \infty$ limit of geodesics may be thought of as arising because one is taking *the limit*. However, this is not the case in the following sense. Given any positive, finite $\tilde{E}$, one can always find a null geodesic with sufficiently large but *finite* L that emanates from the white hole, briefly exits the horizon, and

[7] Identification with the white hole of the *same* solution is also a mathematical possibility, though that would create closed timelike curves within the spacetime, considered by some a class of 'pathology' more severe than the black/white hole singularity.

then returns to the black hole, and in doing so orbits *arbitrarily* close to 2π radians in azimuth, and completes the journey in *arbitrarily* small, but non-zero affine time.

Another remark is that understanding the invariant manifolds and unstable hyperbolic points allows standard techniques to be used to show that perturbations of the geodesic flow will generically cause chaotic motion. For example, for this purpose, solutions in T_1 may be regarded as forming a homoclinic loop if we identify p^+ and p^-. Perturbations will then generically break the homoclinic loop and cause chaotic motion by the Smale–Birkhoff theorem [17].

Even though we restricted attention to null geodesics for simplicity, we expect that similar mappings could be used for timelike particles, or more complicated geometries like Kerr. This would be an interesting avenue for future work.

Acknowledgments

We would like to thank T Hinderer, I Rodnianski, D Spergel for helpful discussions. This work was supported by the Alfred P Sloan Foundation (FP), NSF grant PHY-0745779 (FP) and NASA/AISR grant NNX09AK61G (EB).

References

[1] Levin J and Perez-Giz G 2008 *Phys. Rev.* D **77** 103005
[2] Levin J and Perez-Giz G 2009 *Phys. Rev.* D **79** 124013
[3] Perez-Giz G and Levin J 2009 *Phys. Rev.* D **79** 124014
[4] Moeckel R 1992 *Commun. Math. Phys.* **150** 415
[5] Vieira W M and Letelier P S 1996 *Phys. Rev. Lett.* **76** 1409
Vieira W M and Letelier P S 1996 *Phys. Rev. Lett.* **76** 4098 (erratum)
[6] Letelier P S and Vieira W M 1997 *Class. Quantum Grav.* **14** 1249
[7] Cornish N J and Frankel N E 1997 *Phys. Rev.* D **56** 1903
[8] Suzuki S and Maeda K i 2000 *Phys. Rev.* D **61** 024005
[9] de Moura A P S and Letelier P S 2000 *Phys. Rev.* E **61** 6506
[10] Saa A and Venegeroles R 1999 *Phys. Lett.* A **259** 201
[11] McGehee R 1981 *Comment. Math. Helv.* **56** 524
[12] Stoica C and Mioc V 1997 *Astrophys. Space Sci.* **249** 161
[13] Kerr R P and Schild A 1965 A new class of vacuum solutions of the Einstein field equations *Proc. Galileo Galilei Centenary Meeting on General Relativity, Problems of Energy and Gravitational Waves* ed G Barbera (Florence, Comitato Nazionale per le Manifestazione Celebrative, 1965) p 222
[14] Eddington A S 1924 *Nature* **113** 192
[15] Finkelstein D 1958 *Phys. Rev.* **110** 965
[16] Marck J A 1996 *Class. Quantum Grav.* **13** 393
[17] Belbruno E 2004 *Capture Dynamics and Chaotic Motions in Celestial Mechanics* (Princeton, NJ: Princeton University Press)